In-line phase modulators using coaxial thick lead zirconate titanate coated optical fibers

Barrow, D. A.; Lisbôa, O.; Jen, C. K.; Sayer, M.

Publisher's version / Version de l'éditeur:
https://doi.org/10.1063/1.362661
Journal of Applied Physics, 79, 6, pp. 3323-3329, 1996-03-15

Journal of Applied Physics

RESEARCH ARTICLE | MARCH 15 1996

In-line phase modulators using coaxial thick lead zirconate titanate coated optical fibers

D. A. Barrow; O. Lisbôa; C. K. Jen; M. Sayer

Journal of Applied Physics 79, 3323–3329 (1996)
https://doi.org/10.1063/1.362661

AIP Publishing

In-line phase modulators using coaxial thick lead zirconate titanate coated optical fibers

D. A. Barrow
Department of Physics, Queen's University, Kingston, Ontario K7L 3N6, Canada

O. Lisbôa
Department of Electrical Engineering, McGill University, Montreal, Quebec H3A 2A7, Canada

C. K. Jen[a)]
IMI, National Research Council, Boucherville, Quebec J4B 6Y4, Canada

M. Sayer
Department of Physics, Queen's University, Kingston, Ontario K7L 3N6, Canada

(Received 25 August 1995; accepted for publication 22 November 1995)

Thick piezoelectric lead zirconate titanate (PZT) films (ceramic–ceramic 0–3 composite films), using a new sol-gel based process, have been produced and used to coaxially coat optical fibers. Coated PZT of up to 200 μm thick and 10 cm long have been achieved. Using thick PZT coated single mode optical fibers, in-line phase modulators are designed, built and tested. Theoretical and experimental investigations of such phase modulators are also presented. The measured phase modulation ranges from hundreds of kilohertz to several megahertz. © *1996 American Institute of Physics.* [S0021-8979(96)05605-X]

I. INTRODUCTION

In-line optical fiber components such as phase modulators, which can be used to manipulate the guided light directly within the optical fiber, are of interest in optical fiber communication networks and sensors.[1,2] A common component used for phase modulation in optical fiber interferometers is a piezoelectric cylinder tube wrapped around by many turns of optical fiber under a small tension.[3,4] Although this kind of phase modulator is very efficient, it suffers several drawbacks (e.g., size, weight, etc.), and can be used only at low frequencies (a few kilohertz). Several other kinds of in-line fiber phase modulators, such as fibers with coaxial piezoelectric transducers,[5] fibers with piezoelectric plastic jackets [polyvinyledene difluoride (PVDF), lead zironate titanate (PZT) composites, etc.],[6–9] have been reported. Although the piezoelectric plastic jackets can provide phase modulation in relatively high frequencies (a few megahertz), their efficiencies are relatively low due to their low piezoelectricity and poor acoustic impedance match between the plastics and silica fibers. More recently, even higher frequency phase modulators, which use a piezoelectric thin film directly deposited onto a short section of fiber (a few millimeters), have been studied.[10,11] The preferred choice for the piezoelectric thin film was the oriented zinc oxide (ZnO). Phase modulators with operating frequencies around a few hundreds of megahertz have been demonstrated using ZnO thin films.[10] But the deposition of such films with the proper orientation on a long cylindrical surface is one of the major difficulties of this technology.[11] The substrate must also be heated above 250 °C inside the vacuum chamber and glass is not a good thermal conductor. It is also difficult to make thick ZnO films for low frequency operations.

In this article an alternative in-line fiber phase modulator using a thick PZT coated single-mode fiber is presented. In this device, the phase modulation is achieved by properly exciting the thick PZT coating so that it works as an ultrasonic transducer. The thick PZT coating is produced by using a new sol-gel based process developed in our laboratories. Since the thickness of the PZT films can be controlled and defined by using this process, the optical phase modulator can be designed to operate in a relatively large frequency range, hundreds of kilohertz to several megahertz, which are suitable for phase adjustments in several optical fiber interferometers. Also, the efficiency which may be obtained with this device is theoretically about two orders of magnitude higher than that obtained with piezoelectric plastic jacket films mentioned previously.

II. BASIC PRINCIPLES

A. Sol-gel process

Sol-gel processing of ceramic films has been attractive for both electrical and structural applications. Besides producing ceramic films with similar characteristics to the corresponding bulk ceramic materials, the sol-gel process is generally simple and can coat complex shapes. A wide range of ceramic coatings have been fabricated on a variety of substrate materials and shapes.[12–14] Ceramic coatings such as zirconia and alumina are sought after in applications requiring dense, high quality films for protection against oxidation and corrosion as well as for thermal barrier coatings. In terms of electrical device applications, PZT films have attracted interest in dielectric, ferroelectric, and piezoelectric,[15,16] device applications.

In the sol-gel process, films are fabricated from mixed solutions of their metallorganic compounds dissolved in a suitable solvent. The obtained solution is first hydrolyzed to form a structured solution, or gel, containing polymers, or

[a)]Electronic mail: cheng-kuei.jen@nrc.ca

macroclusters. Also, additives are used to control the viscosity and surface tension of the sol-gel solution. Films can be formed by spin, dip, or spray coating onto appropriate substrates. The organic portion of the film is removed by heating. Finally, a subsequent heat treatment is usually required to fully develop the final ceramic structure.

B. Sol-gel process for the fabrication of thick PZT coatings

Presently, the main limitation in sol-gel processing has been the film thickness that is achievable. It is difficult to fabricate crack-free films >10 μm in thickness. This restricts the potential applications of this process because there are several piezoelectric applications that require thicker films.[17–19]

In our group, a sol-gel based technology[17–20] has been developed for fabricating PZT films of the thicknesses required to address some of these applications. The films are 0–3 ceramic-ceramic composites and are formed by dispersing ceramic PZT particles in the sol-gel solution.[17,18] This dispersion can be deposited in the same manner as conventional sol-gel and with this process, film thicknesses of up to at least 200 μm can be achieved by coating multiple layers.

The final film is essentially a composite made of two phases of PZT: ceramic PZT particles dispersed in a sol-gel produced PZT matrix. These films can be modeled as 0–3 composites using the theory outlined by Newnham *et al.*[21] for polymeric PZT composites. However, an advantage of the ceramic-ceramic composite films presented in this article is that both phases of the composite are highly piezoelectric and consequently electrical properties of the resulting film are comparable to those of the bulk ceramic. Preliminary analysis of the dielectric constant using 0–3 composite theory has previously been reported.[19]

In order to fabricate in-line fiber optic modulators, thick PZT films were coaxially deposited onto aluminum jacket single mode optical fibers using this process. Including the aluminum jacket ($\approx$30 μm thick), the total outer diameter of the optical fiber used was $\sim$185 μm. These fibers were commercially obtained from Fiberguide Industries (Stirling, NJ). In order to integrate the coated optical fiber into a fiber optic interferometric sensor for testing, it was necessary to develop a special coating procedure to deposit the PZT film in the middle of a section of the fiber. Namely after cleaning the fiber, a few drops of the dispersion was dropped onto a metallic ring which supports a meniscus of the solution as shown in Fig. 1. The ring with the PZT solution was then hooked around the optical fiber. Ceramic PZT powders (BM Hi-Tech BM 400, Collingwood, Ontario) were dispersed in the solution so that the final fired film consisted of 70% ceramic powder by weight. The high powder loading of the solution made it possible to deposit thick layers in a single coat, however, it also increased the porosity of the film. Then a computer controlled stepper motor holding the optical fiber moved vertically through the ring at a controlled rate of 5 cm/min, for the desired length. 5 μm thick films were deposited in a single layer. After the coating stage, the fiber was moved to a furnace to dry the deposited coating. The last two steps were repeated until the required coating thickness was achieved. After the final coating, the PZT coated fiber section was heated at 650 °C for 5 h to fully crystallize the material. In the final processing stage, a top electrode was deposited on the circumference of the PZT film and piezoelectricity was induced by applying an appropriate poling voltage (typically 30 kV/cm) at 200 °C between the inner and outer electrodes. Figure 2 shows a cross-sectional micrograph of an $\approx$200 μm PZT film coaxially deposited onto the optical fiber mentioned.

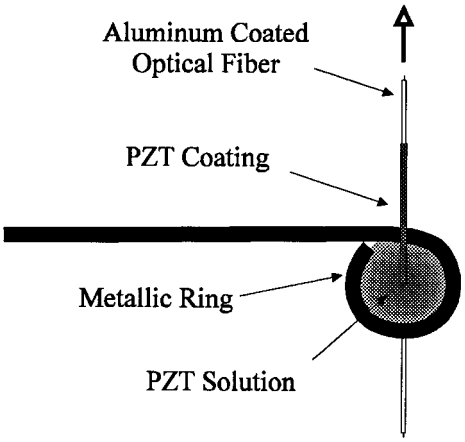

FIG. 1. Schematic of the metallic ring, which supports a meniscus of the PZT solution, used in the process for coating the optical fiber.

C. In-line fiber phase modulator

A strand of optical fiber with a 10 cm long section coated coaxially with a piezoactive PZT film of 200 μm thick was then used as an in-line fiber phase modulator. The schematic of the designed in-line fiber phase modulator is

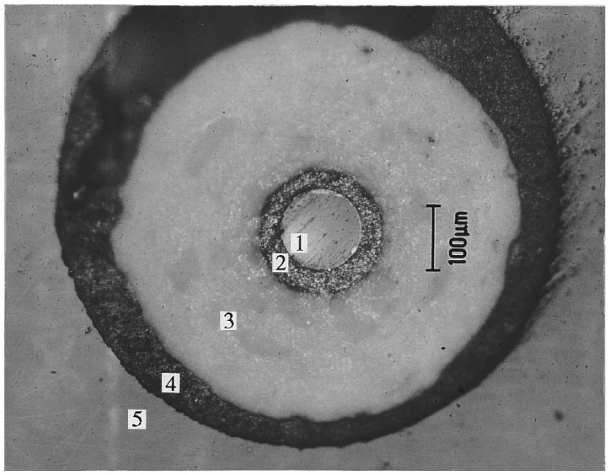

FIG. 2. Cross-sectional micrograph of an $\approx$200 μm PZT film coaxially deposited onto a metallic jacket single-mode optical fiber. 1: Optical fiber, 2: $\approx$30 μm Al jacket, 3: $\approx$200 μm PZT film, 4: Epoxy, 5: Holder.

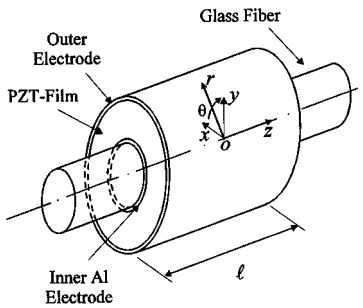

FIG. 3. Schematic of the multilayer structure, and the cylindrical coordinate system for displacement, stress and strain components in the structure.

shown in Fig. 3. As is shown, an aluminum-coated single-mode optical fiber was used. One electric contact was the inner aluminum jacket, and the other electric contact was a metallic coating deposited over the PZT coating. A proper rf signal applied across these two electrodes will induce an optical phase shift (modulation) in the optical beam propagating inside the optical fiber via the length change effect, and also via the refractive index change effect. The phase change can be represented as

$$\Delta\varphi=\frac{2\pi}{\lambda_0}(l\Delta n+n_{\mathrm{eff}}\Delta l), \tag{1}$$

where λ_0 is the free space optical wavelength of the laser, n_{eff} is the effective refractive index of the optical mode guided in the fiber, and l is the length of the optical fiber inside the PZT film.

III. THEORETICAL ANALYSIS

A theoretical analysis for the optical phase shift induced on the light propagating inside the optical fiber coated with a vinylidene fluoride and trifluoroethylene copolymer (VDF/TrFE) film has been reported in Ref. 7. A similar analysis is presented in this section for a PZT coated fiber for the sake of completeness. The designed device is considered as an axisymmetric multilayer structure operating in a radially resonant mode. This multilayer device as shown in Fig. 3 consists of an optical fiber coated with a 30 μm aluminum film used as the inner electrode; a PZT film as the piezoelectric layer; and another aluminum film used as the outer electrode. Figure 3 also shows the cylindrical coordinate system for displacement, stress, and strain components in the structure.

In the theoretical model it is assumed that the device is operated in the axially constrained regime (high frequency), where the longitudinal dimension of the device (in all three layers) is much greater than the wavelength of the extensional elastic wave guided in the structure.[22] In this case, the structure can be considered as an infinitely long cylinder, which means that the strain induced by the PZT film into the fiber is independent of the axial position. Also, the axially symmetric configuration of each layer makes the elastic response azimuthally independent. Using the index ellipsoid formalism in an isotropic material one can find

$$\Delta n=-\frac{n^3}{2}(p_{11}S_1+p_{12}S_2+p_{12}S_3), \tag{2}$$

where p_{11} and p_{12} are the strain-optic tensor components, n is the refractive index of the optical fiber, and $S_{1,2,3}$ are the components of the strain tensor $\tilde{\mathbf{S}}$ induced onto the optical fiber. The components of the strain tensor are given with a consideration of the principal strains (S_1,S_2, and S_3), in an orthogonal axes system with S_3 along the propagation axis of the optical fiber. Therefore, from Eqs. (1) and (2), the optical phase shift in the axially constrained regime, where $\Delta l=0$ and so S_3, can be given by[7]

$$\Delta\varphi=-\frac{2\pi}{\lambda_0}l\frac{n^3}{2}(p_{11}S_1+p_{12}S_2). \tag{3}$$

In our case, for a radially symmetrical strain field, where $S_1=S_2=S_r$, Eq. (3) is rewritten as

$$\Delta\varphi=-\frac{2\pi}{\lambda_0}l\frac{n^3}{2}(p_{11}+p_{12}). \tag{4}$$

The strain in the radial direction, S_r, in a cylindrical coordinate system, for a multilayer structure, is given by

$$S_r^{(i)}=\frac{du_r^{(i)}}{dr}, \tag{5}$$

where $i=1,2,3,4$ represents the strain in the glass fiber ($0\leqslant r\leqslant a$), inner electrode ($a\leqslant r\leqslant b$), PZT film ($b\leqslant r\leqslant c$), and outer electrode ($c\leqslant r\leqslant d$), respectively, as shown in Fig. 3. $u_r^{(i)}$ is the particle displacement $\mathbf{u}^{(i)}(r,\theta,zt)$ in the radial direction.

The particle displacement and the stress in the radial direction satisfies

$$\rho^{(i)}\frac{\partial_2\mathbf{u}^{(i)}}{\partial t^2}=C_{11}^{(i)}\left(\frac{\partial^2\mathbf{u}^{(i)}}{\partial r^2}+\frac{1}{r}\frac{\partial\mathbf{u}^{(i)}}{\partial r}-\frac{\mathbf{u}^{(i)}}{r^2}\right) \tag{6}$$

and

$$\sigma_r^{(i)}(r,t)=C_{11}^{(i)}\frac{\partial\mathbf{u}^{(i)}}{\partial r}+C_{12}^{(i)}\frac{\mathbf{u}^{(i)}}{r}-\frac{e_{11}}{\varepsilon}\mathbf{D}(r,t)\cdot\delta_{i3}, \tag{7}$$

respectively, where $C_{11}^{(i)}$, $C_{12}^{(i)}$, and $\rho^{(i)}$ are the elastic constants and density, respectively, of the ith layer; e_{11} and ε is the piezoelectric stress constant and the permittivity, respectively, of the piezoelectric layer; $\mathbf{D}(r,t)$ is the electric displacement vector; and $\boldsymbol{\delta}_{i3}$ is a Kronecker's delta. The third component in the right-hand side of Eq. (7) represents the piezoelectric stress of the PZT film.

Assuming a separation of variables type of solution for Eq. (6) in the radial direction, i.e.,

$$\mathbf{u}^{(i)}(r,t)=U^{(i)}(r)\cdot e^{j\omega t}\hat{r}, \tag{8}$$

and substituting Eq. (8) into Eqs. (6) and (7) one obtains

$$\frac{d^2U^{(i)}}{dr^2}+\frac{1}{r}\frac{dU^{(i)}}{dr}+\left(\omega^2\frac{\rho^{(i)}}{C_{11}^{(i)}}-\frac{1}{r^2}\right)U^{(i)}=0, \tag{9}$$

and

$$\sigma_r^{(i)}(r)=C_{11}^{(i)}\frac{dU^{(i)}}{dr}+C_{12}^{(i)}\frac{U^{(i)}}{r}-\left(\frac{e_{11}}{\varepsilon}D(r)\right)_{i=3}. \tag{10}$$

TABLE I. Physical constants for the three materials used in the multilayer structure.

	PZT	Electrodes (aluminum)	Optical fiber (fused silica)
Elastic constants $(N/m)^2$	$C_{11}=1.26\times10^{11}$ $C_{12}=7.95\times10^{10}$	$C_{11}=1.10\times10^{11}$ $C_{12}=5.81\times10^{10}$	$C_{11}=7.85\times10^{10}$ $C_{12}=1.61\times10^{10}$
Density (kg/m^3)	$\rho=7.50\times10^3$	$\rho=2.69\times10^3$	$\rho=2.20\times10^3$
Relative permittivity $(\varepsilon/\varepsilon_0)$[a]	$\varepsilon_r=1470$	⋯	⋯
Piezoelectricity (C/m^2)	$e=23.3$	⋯	⋯

[a]ε_0 is the permittivity of vacuum.

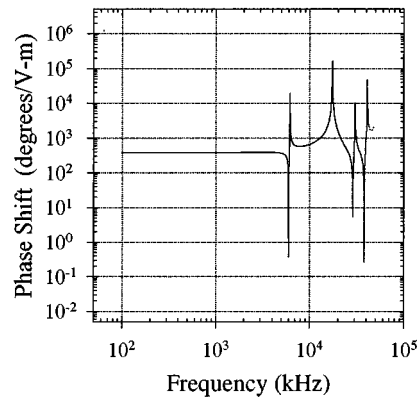

FIG. 4. Calculated frequency response of the basic in-line fiber phase modulator. PZT film thickness ≈120 μm.

Assuming that the electric displacement in the PZT film decreases with the radial distance from the geometric center we have

$$D(r)=\frac{D_0}{r}, \tag{11}$$

where D_0 is a constant. Therefore the differential [Eq. (9)] is satisfied provided that the particle displacement in the radial direction is given by a combination of the first-order Bessel functions as

$$U^{(i)}(r)=A^{(i)}J_1(g^{(i)}r)+B^{(i)}Y_1(g^{(i)}r), \tag{12}$$

where $A^{(i)}$ and $B^{(i)}$ are the unknown coefficients of the ith layer's displacement of the compressional acoustic wave, and $g^{(i)}=\omega(\rho^{(i)}/C_{11}^{(i)})^{1/2}$. In order to find the coefficients $A^{(i)}$ and $B^{(i)}$, the boundary conditions for Eqs. (10) and (12) are: (a) $U(r=0)=0$, (b) continuity of U and σ_r at each interface inside the multilayer structure, and (c) $\sigma_r\ (r=d)=0$. From (a), $B^{(i)}=0$, and from (b) and (c), we obtain a simultaneous equation system written in matrix form as

$$\begin{bmatrix} a_{11} & \cdot & \cdot & \cdot & a_{17} \\ \cdot & \cdot & & & \cdot \\ \cdot & & \cdot & & \cdot \\ \cdot & & & \cdot & \cdot \\ a_{71} & \cdot & \cdot & \cdot & a_{77} \end{bmatrix} \begin{bmatrix} A^{(1)} \\ A^{(2)} \\ B^{(2)} \\ A^{(3)} \\ B^{(3)} \\ A^{(4)} \\ B^{(4)} \end{bmatrix} = \begin{bmatrix} b_1 \\ \cdot \\ \cdot \\ \cdot \\ b_7 \end{bmatrix}, \tag{13}$$

where a_{ij} and b_i are given in the Appendix. Once Eq. (13) is solved, the coefficients $A^{(i)}$ and $B^{(i)}$ are known and, from Eq. (5), the radial distribution of the strain in each layer can be found. Finally, the optical phase shift induced into the optical mode by the PZT film is obtained from Eq. (4), with $S_r=S_r^{(1)}(r=0)$.

IV. THEORETICAL RESULTS

To calculate the optical phase shift induced by the PZT film certain physical constants for the three materials used in the multilayer structure are required. Table I shows all data necessary in the equations to obtain the optical phase shift induced by the PZT film.

The theoretical behavior of the phase modulator was evaluated by considering the thickness of the layers as 62.5, 30, 120, and 10 μm for the optical fiber, the inner electrode, the PZT film and the outer electrode, respectively. Further on, the phase modulator with this particular set of parameters will be referred to as the *basic* device. Figure 4 shows the theoretical frequency response of this basic device, where the phase shift is given in a normalized unit (deg/V m). The value of the phase shift in the flat region of the curve (from ≈100 kHz to ≈5.8 MHz) is $\Delta\varphi\approx382$ (deg/V m), indicating that theoretically the device has a very high efficiency in comparison with other similar devices which use PVDF and ZnO as the piezoelectric active layer in their structure.[7–10] Specifically, the piezoelectric constants of piezoelectric polymers are in general two orders of magnitude lower than those of the ceramic PZT materials. Thus, typical theoretical values for the phase shifts obtained with the piezoelectric polymer coated fiber phase modulators are also about two orders of magnitude lower than those evaluated in the PZT coated device.

In Fig. 4 each relative maximum peak of phase shift corresponds to a radial resonance phenomenon of the multilayer structure. The peaks at the relative minimum phase shifts, correspond to a radial antiresonance phenomenon. At antiresonance frequencies the radial displacements in the optical fiber are virtually zero and do not induce any phase shift into the light passing through the modulator. One can see that the first radial antiresonance happens at a lower frequency than the first radial resonance. However, if the thickness of the PZT film is <110 μm, our theoretical results show that the first radial resonance will appear before the radial antiresonance.

V. EXPERIMENTAL RESULTS

In-line fiber phase modulators were fabricated according to the dimensions and materials defined in Sec. IV (referred to as the basic device) including a coating length $l=4.8$ cm, with one exception that the material of the outer electrode was a 10 μm thick conducting silver paste. Silver paste was selected because of the simplicity to obtain a conductive coating around the entire PZT-coated fiber section and its

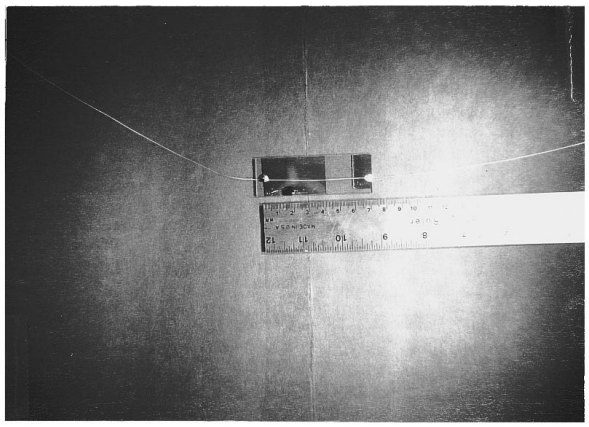

FIG. 5. Picture of a typical in-line fiber phase modulator implemented.

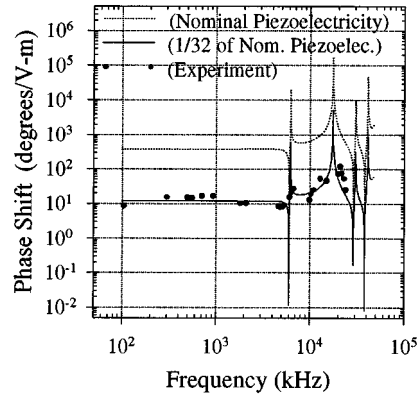

FIG. 7. Frequency response of the in-line fiber phase modulator implemented for measurements (solid dots). The plot represented by the solid line is the theoretical frequency response of the device if the piezoelectric constant of the PZT film was reduced to 1/32 of its nominal value. The plot represented by the dashed line is the same plot shown in Fig. 4, where the piezoelectric constant of the PZT film is equal to its original nominal value.

effects on the performance of the designed basic phase modulator are not significant in the frequency range of interest. Figure 5 shows a close view of a typical device used in the experiments.

For evaluating the experimental behavior of the phase modulator mentioned above, a fiber optic Mach–Zehnder interferometer, whose schematic is shown in Fig. 6, was set up. The phase shift was measured using the so-called $J_1,\ldots,J_4$ method.[23] The data obtained from the measurements are plotted in Fig. 7 as the solid dots. As mentioned earlier, at present, the fabricated thick PZT coating exhibits high porosity due to the high PZT powder concentration (70% by weight) dispersed in the solution. This high porosity leads not only to a high ultrasonic attenuation but also to a lower piezoelectricity. Although our process could produce dense films if the powder concentration is kept in a certain range. However, as the powder concentration in the film increases the porosity also rises because there is not enough solution to fill in the gaps. Again, a high powder concentration was used so that thick films in this work could be easily achieved. This was also required due to the surface roughness of the outer aluminum jacket on the optical fiber. Better densities could be achieved by reducing the powder concentration and this would be carried out in the future.

The low piezoelectricity activity was caused by two additional factors. First, the processing was not optimized in terms of the firing temperature. It may be that organic material remains trapped in the film thus reducing the piezoelectric properties. The processing has to be investigated further. Second, an insulating oxide layer that forms in the aluminum/PZT interface reduces the effective voltage applied across the PZT film.

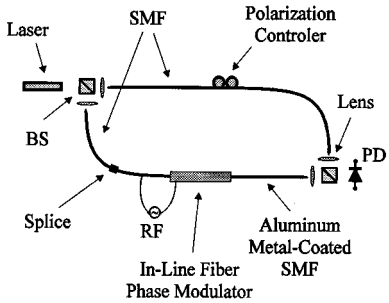

FIG. 6. Schematic of the fiber optic Mach–Zehnder interferometer built to measure the phase shift induced by the in-line fiber phase modulator. SMF (single-mode fiber); BS (beamsplitter); PD (photodetector).

In order to compare the theoretical results obtained with the experimental data measured from the device in the frequency domain, we arbitrarily reduce the piezoelectric constant of the PZT film to 1/32 of its nominal value in the theoretical calculation which is indicated as the solid line in Fig. 7. Clearly, we can see that there is a good agreement in the resonant behaviors in the frequency spectrum. The dashed line in Fig. 7 is the same plot shown in Fig. 4 that represents the frequency response of the basic designed device where the piezoelectric constant of the PZT film was considered equal to its original nominal value.

Furthermore, the high dielectric constant of the PZT film induces a high capacitance along the long length of PZT-coated fiber section. At high MHz frequency range the Q value of the device decreases as its capacitance increases. Thus the experimental resonance peaks do not respond sharply because of the low Q caused by the impedance mismatching between the modulator and the 50Ω output impedance of the signal generator which drives the modulator. This factor was not included in the theoretical considerations. The high capacitance which is proportional to the inverse of the thickness was also the main and critical reason that thick PZT coatings were preferred over the thin ones for the fabrication of the phase modulator operated in the frequency range of our interests (less than a few MHz). The remedy for this capacitance effect may be achieved by electrically connecting multisections of PZT-coated fiber in series.

Finally, the solid dots in Fig. 8 represent the induced phase shift of the experimental device versus the applied voltage driving at 108 kHz which was arbitrarily chosen. The least-squares fit of the results is also shown in Fig. 8 as a

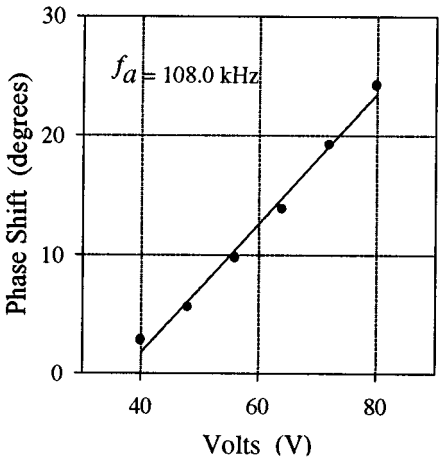

FIG. 8. Induced phase shift vs the applied voltage driving at 108 kHz. Solid dots are the measured results. The solid line represents the least-squares fit of the results, and points out a linear behavior of the device within the range of the applied voltage.

solid line which points out a linear behavior of the phase modulator within the range of the applied voltage.

VI. CONCLUSION

In this article we introduced a sol-gel based process to produce coaxial thick piezoelectric lead zirconate titanate (PZT) coatings on optical fibers. PZT films of thickness up to 200 μm and length up to 10 cm have been achieved. This device was later used as an in-line fiber phase modulator. Since PZT has high dielectric constants and the high efficiency of the phase modulation at the frequency of our interest desires low capacitance, thick film was then chosen. It is well understood that the thicker the film, the lower the capacitance.

A theoretical analysis for the optical phase modulation induced by the PZT film on the light propagating inside the optical fiber was presented. The theory was based on an axisymmetrical multilayer structure operated in radially resonant mode. The measured phase modulation induced by the radial acoustic modes ranged from 100 kHz to 25 MHz. Experimental results showed that the frequency response of the phase modulator was in good agreement with the theoretical predictions; however, the efficiency of the device is much lower than that obtained in the theoretical calculation. This lower efficiency was due to fact that the thick PZT film deposited on the optical fiber exhibited high porosity which led not only to a high ultrasonic attenuation but also to a lower piezoelectricity. Further improvements in the fabrication process, characterization of the thick PZT films and device designs are needed in order to produce practical in-line fiber devices such as phase modulators.

ACKNOWLEDGMENTS

Financial support from the Natural Sciences and Engineering Research Council of Canada and the Ontario Centre for Materials Research is appreciated. O. Lisbôa would like to thank CTA/COBAE/MECB-Brazil, and CNPq-Brazil for financial support and fellowship.

APPENDIX

The matrix elements a_{ij} and b_i of Eq. (13) are

$$a_{11}=[C_{11}^{(1)}g^{(1)}J_0(g^{(1)}a)-C_{11}^{(1)}/aJ_1(g^{(1)}a)+C_{12}^{(2)}/aJ_1(g^{(1)}a)], \tag{A1}$$

$$a_{12}=-[C_{11}^{(2)}g^{(2)}J_0(g^{(2)}a)-C_{11}^{(2)}/aJ_1(g^{(2)}a)+C_{12}^{(2)}/aJ_1(g^{(2)}a)], \tag{A2}$$

$$a_{13}=-[C_{11}^{(2)}g^{(2)}Y_0(g^{(2)}a)-C_{11}^{(2)}/aY_1(g^{(2)}a)+C_{12}^{(2)}/aY_1(g^{(2)}a)], \tag{A3}$$

$$a_{14}=a_{15}=a_{16}=a_{17}=0, \tag{A4}$$

$$a_{21}=J_1(g^{(1)}a), \quad a_{22}=-J_1(g^{(2)}a),$$

$$a_{23}=-Y_1(g^{(2)}a), \tag{A5}$$

$$a_{24}=a_{25}=a_{26}=a_{27}=0, \tag{A6}$$

$$a_{31}=a_{36}=a_{37}=0, \tag{A7}$$

$$a_{32}=[C_{11}^{(2)}g^{(2)}J_0(g^{(2)}b)-C_{11}^{(2)}/bJ_1(g^{(2)}b)+C_{12}^{(2)}/bJ_1(g^{(2)}b)], \tag{A8}$$

$$a_{33}=[C_{11}^{(2)}g^{(2)}Y_0(g^{(2)}b)-C_{11}^{(2)}/bY_1(g^{(2)}b)+C_{12}^{(2)}/bY_1(g^{(2)}b)], \tag{A9}$$

$$a_{34}=-[C_{11}^{(3)}g^{(3)}J_0(g^{(3)}b)-C_{11}^{(3)}/bJ_1(g^{(3)}b)+C_{12}^{(3)}/bJ_1(g^{(3)}b)], \tag{A10}$$

$$a_{35}=-[C_{11}^{(3)}g^{(3)}Y_0(g^{(3)}b)-C_{11}^{(3)}/bY_1(g^{(3)}b)+C_{12}^{(3)}/bY_1(g^{(3)}b)], \tag{A11}$$

$$a_{41}=a_{46}=a_{47}=0, \tag{A12}$$

$$a_{42}=J_1(g^{(2)}b), \quad a_{43}=Y_1(g^{(2)}b),$$

$$a_{44}=-J_1(g^{(3)}b), \quad a_{45}=-Y_1(g^{(3)}b), \tag{A13}$$

$$a_{51}=a_{52}=a_{53}=0, \tag{A14}$$

$$a_{54}=[C_{11}^{(3)}g^{(3)}J_0(g^{(3)}b)-C_{11}^{(3)}/cJ_1(g^{(3)}c)+C_{12}^{(3)}/cJ_1(g^{(3)}b)], \tag{A15}$$

$$a_{55}=[C_{11}^{(3)}g^{(3)}Y_0(g^{(3)}c)-C_{11}^{(3)}/cY_1(g^{(3)}c)+C_{12}^{(3)}/cY_1(g^{(3)}c)], \tag{A16}$$

$$a_{56}=-[C_{11}^{(4)}g^{(4)}J_0(g^{(4)}c)-C_{11}^{(4)}/cJ_1(g^{(4)}c)+C_{12}^{(4)}/cJ_1(g^{(4)}c)], \tag{A17}$$

$$a_{57}=-[C_{11}^{(4)}g^{(4)}Y_0(g^{(4)}c)-C_{11}^{(4)}/cY_1(g^{(4)}c)+C_{12}^{(4)}/cY_1(g^{(4)}c)], \tag{A18}$$

$$a_{61}=a_{62}=a_{63}=0, \tag{A19}$$

$$a_{64}=J_1(g^{(3)}c), \quad a_{65}=Y_1(g^{(3)}c),$$

$$a_{66}=-J_1(g^{(4)}c), \quad a_{67}=-Y_1(g^{(4)}c), \tag{A20}$$

$$a_{71}=a_{72}=a_{73}=a_{74}=a_{75}=0, \tag{A21}$$

$$a_{76}=[C_{11}^{(4)}g^{(4)}J_0(g^{(4)}d)-C_{11}^{(4)}/dJ_1(g^{(4)}d)+C_{12}^{(4)}/dJ_1(g^{(4)}d)], \tag{A22}$$

$$a_{77}=[C_{11}^{(4)}g^{(4)}Y_0(g^{(4)}d)-C_{11}^{(4)}/dY_1(g^{(4)}d)+C_{12}^{(4)}/dY_1(g^{(4)}d)], \tag{A23}$$

$$b_{11}=b_{21}=b_{41}=b_{61}=b_{71}=0, \tag{A24}$$

$$b_{31}=-\frac{e_{11}}{\varepsilon b}D_0, \quad b_{35}=\frac{e_{11}}{\varepsilon c}D_0. \tag{A25}$$

[1] R. P. De Paula and E. L. Moore, Proc. SPIE **478**, 3 (1984).
[2] R. H. Stolen and R. P. De Paula, Proc. IEEE **75**, 1498 (1987).
[3] D. E. N. Davies and S. A. Kingsley, Electron. Lett. **10**, 21 (1974).
[4] S. A. Kingsley, Electron. Lett. **14**, 419 (1978).
[5] S. A. Kingsley, Electron. Lett. **11**, 453 (1975).
[6] M. Imai, H. Tanizawa, Y. Ohtsuka, Y. Takase, and A. Odajima, J. Appl. Phys. **60**, 1916 (1986).
[7] M. Imai, T. Yano, K. Motoi, and A. Odajima, J. Quantum Electron. **28**, 1901 (1992).
[8] E. F. Carome and K. P. Koo, IEEE Ultrason. Symp. **US-2**, 710 (1980).
[9] J. Jarzynski, J. Appl. Phys. **55**, 3243 (1984).
[10] D. S. Czaplak, J. F. Weller, L. Goldberg, F. S. Hickernell, H. D Knuth, and S. R. Young, IEEE Ultrason. Symp. **US-1**, 491 (1987).
[11] B. L. Heffner, W. P. Risk, B. T. Khuri-Yakub, and G. S. Kino, IEEE Ultrason. Symp. **US-2**, 709 (1986).
[12] M. Sayer, IEEE Ultrason. Symp. **1**, 595 (1991).
[13] C. K. Jen, M. Sayer, G. Yi, and J. F. Bussiére, U. S. Patent No. 5,135,295 (4 August 1992).
[14] P. K. Larsen, G. L. M. Kampschöer, M. J. E. Ulenaers, G. A. C. M. Spierings, and R. Cuppens, Appl. Phys. Lett. **59**, 611 (1991).
[15] M. Sayer, Integrated Ferroelect. **1**, 151 (1992).
[16] D. L. Polla, P. J. Schiller, and L. F. Francis, Proc. SPIE **2291**, 108 (1994).
[17] D. A. Barrow, Ph. D. dissertation, Kingston, Ontario, June 1995.
[18] D. A. Barrow, T. E. Petroff, and M. Sayer, Surf. Coat. Technol. (in press, 1996).
[19] D. A. Barrow, R. P. Tandon, T. E. Petroff, and M. Sayer, J. Appl. Phys. (in press, 1996).
[20] D. A. Barrow, T. E. Petroff, and M. Sayer, U. S. Patent application (1995).
[21] R. E. Newnham, D. T. Skinner, and L. E. Cross, Mater. Res. Bull. **13**, 525 (1978).
[22] R. P. De Paula, J. Jarzynsky, C. C. Ku, J. A. Bucaro, and J. H. Cole, Proc. SPIE **425**, 111 (1983).
[23] V. S. Sudarshanam and K. Srinivasan, Opt. Lett. **14**, 140 (1989).